A High-Efficiency Fiber-to-Waveguide Coupler with Low Polarization Dependence Using a Diluted Waveguide in InP Substrate with a 1.55μm Wavelength*

Zhang Yun, Zuo Yuhua†, Guo Jianchuan, Ding Wuchang, Cheng Buwen, Yu Jinzhong, and Wang Qiming

(*State Key Laboratory of Integrated Optoelectronics, Institute of Semiconductors, Chinese Academy of Sciences, Beijing* 100083, *China*)

Abstract: We propose a fiber-to-waveguide coupler for side-illuminated p-i-n photodiodes to obtain high responsivity and low polarization dependence that is grown on InP substrate and is suitable for surface hybrid integration in low cost modules. The fiber-to-waveguide coupler is based on a diluted waveguide, which is composed of ten periods of undoped 120nm InP /80nm InGaAsP (1.05μm bandgap) multiple layers. Using the semi-vectorial three dimensional beam propagation method (BPM) with the central difference scheme, the coupling efficiency of fiber-to-waveguide under different conditions is simulated and studied, and the optimized conditions for fiber-to-waveguide coupling are obtained. For TE-like and TM-like modes, the calculated maximum coupling efficiency is higher than 94% and 92%, respectively. The calculated polarization dependence is less than 0.1dB, showing good polarization independence.

Key words: diluted waveguide; BPM; fiber-to-waveguide; waveguide photodiode
PACC: 4281M **EEACC**: 4130
CLC number: O472$^+$.3 **Document code**: A **Article ID**: 0253-4177(2008)01-0055-08

1 Introduction

Compared with the surface-illuminated photodiodes, side-illuminated photodiodes have a special advantage: there is no tradeoff between quantum efficiency and bandwidth. This means that they can overcome the tradeoff limitation with the side-illuminated photodiodes to obtain high responsivity and high bandwidth at the same time. Waveguide photodiodes with an external quantum efficiency of greater than 80% and 3dB bandwidth of greater than 50GHz, which is side-illuminated, have been reported[1]. The main problem of such detectors is coupling the light from a fiber to the detectors with high efficiency and low polarization dependence[2]. A great deal of structures have been proposed and fabricated such as tapers[3] and grating couplers[4]. Using these approaches, the side-illuminated photodiodes may gain high responsivity, but at the expense of complicating fabrication[5]. Diluted waveguides with different epitaxial layers have been adopted as the fiber-to-waveguide coupler in the evanescently coupled side-illuminated photodiodes and waveguide p-i-n photodiodes[1,5~10]. A diluted waveguide coupler, composed of ten periods of undoped 100nm/80nm InP/InGaAsP (Q1.1μm), with a coupling efficiency of more than 82% and polarization dependence of less than 0.5dB has been realized[5]. Recently, a coupling efficiency of higher than 90% for a diluted waveguide coupler composed of seven InGaAsP (Q1.07μm) layers with 50, 80, 110, 140, 170, 200, and 580nm thicknesses, interspersed between the 150nm-thick InP layer, with a polarization dependence less than 0.8dB has been demonstrated[10]. Our approach uses ten periods of undoped 120nm/80nm InP/InGaAsP (Q1.05μm) planar diluted waveguide as the fiber-to-waveguide coupler. In this paper, the simulation and optimization of the coupler are described in detail, not only for the diluted waveguide, but also for the lensed fiber. The BPM algorithm is introduced, and mathematical formulations for the full and semi vector BPM are established and discussed. The main equations for the semi-vector BPM in the form of standard alternating direction method (ADI) based on Crank-Nicholson scheme are derived. We explain theoretically why a diluted waveguide is chosen as the fiber-to-waveguide coupler. Using the imaginary distance semi-vector BPM, the whole modes of diluted waveguide with different widths are calculated. The coupling efficiency of fiber-to-waveguide at different conditions is simulated and the optimized conditions for fiber-to-waveguide coupling are obtained.

* Project supported by the National High Technology Research & Development Program of China (No. 2006CB302802)
† Corresponding author. Email: yhzuo@red.semi.ac.cn
Received 9 July 2007, revised manuscript received 21 August 2007

2 The BPM algorithm

Polarization effects can be accounted for by the vector BPM algorithm, and under the slowly varying envelope approximation, we obtain the paraxial vector wave equations in uniform structures[11]:

$$\begin{aligned} \mathrm{j}\frac{\partial E_x}{\partial z} &= A_{xx}E_x + A_{xy}E_y \\ \mathrm{j}\frac{\partial E_y}{\partial z} &= A_{yy}E_y + A_{yx}E_x \end{aligned} \tag{1}$$

where A_{ij} are the complex differential operators, which are defined as:

$$\begin{aligned} A_{xx}E_x &= \frac{1}{2n_0k_0}\left\{\frac{\partial}{\partial x}\left[\frac{1}{n^2}\times\frac{\partial}{\partial x}(n^2E_x)\right]+\frac{\partial^2}{\partial y^2}E_x+(n^2-n_0^2)k_0^2E_x\right\} \\ A_{yy}E_y &= \frac{1}{2n_0k_0}\left\{\frac{\partial}{\partial y}\left[\frac{1}{n^2}\times\frac{\partial}{\partial y}(n^2E_y)\right]+\frac{\partial^2}{\partial x^2}E_y+(n^2-n_0^2)k_0^2E_y\right\} \\ A_{xy}E_y &= \frac{1}{2n_0k_0}\left\{\frac{\partial}{\partial x}\left[\frac{1}{n^2}\times\frac{\partial}{\partial y}(n^2E_y)\right]-\frac{\partial^2}{\partial x\partial y}E_y\right\} \\ A_{yx}E_x &= \frac{1}{2n_0k_0}\left\{\frac{\partial}{\partial y}\left[\frac{1}{n^2}\times\frac{\partial}{\partial x}(n^2E_x)\right]-\frac{\partial^2}{\partial y\partial x}E_x\right\} \end{aligned} \tag{2}$$

k_0 is the wavenumber in free space and n_0 is a constant, chosen as a reference refractive index.

Equation (1) shows that the transverse electric field components are polarization-dependent and coupled with each other. In Eq. (2), the operators A_{xx} and A_{yy} account for polarization dependence due to different boundary conditions at interfaces, and describe such effects as different propagation constants, field distribution, etc. for TE and TM mode. The off-diagonal terms A_{xy} and A_{yx} account for polarization coupling and hybrid modes due to geometric effects, such as those irregular geometric shapes in the cross-sectional structure, and the material anisotropy. The epitaxial structure of the diluted waveguide presented here is a regular shape for isotropy materials, thus the couplings between the two polarizations are quite weak in propagation. The off-diagonal terms A_{xy} and A_{yx} can be neglected, transforming Eq. (1) into:

$$\frac{\partial E_x}{\partial z} = -\mathrm{j}A_{xx}E_x, \quad \frac{\partial E_y}{\partial z} = -\mathrm{j}A_{yy}E_y \tag{3}$$

This is the semi-vector BPM and is precise enough for the diluted waveguide.

With the finite-difference approach based on the central difference scheme, also the well-known Crank-Nicholson scheme, $x = m\Delta x$, $y = n\Delta y$ and $z = l\Delta z$, Equation (3) can be discretized in the following forms[12]:

$$A_{xx}E_x = -\frac{\mathrm{j}}{2n_0k_0}\left\{\frac{T_{m+1,n}E_x(m+1,n)-[2-R_{m+1,n}-R_{m-1,n}]E_x(m,n)+T_{m-1,n}E_x(m-1,n)}{(\Delta x)^2}+\frac{E_x(m,n+1)-2E_x(m,n)+E_x(m,n-1)}{(\Delta y)^2}+[n^2(m,n,l)-n_0^2]k_0^2E_x(m,n)\right\}$$

where T and R are the transmission and reflection coefficients across the index interfaces between $m\Delta x$ and $(m+1)\Delta x$, which are defined as:

$$T_{m,n} = \frac{2n^2(m+1,n,l)}{n^2(m,n,l)+n^2(m+1,n,l)}, R_{m,n} = T_{m,n}-1$$

$$A_{yy}E_y = -\frac{\mathrm{j}}{2n_0k_0}\left\{\frac{T_{m,n+1}E_y(m,n+1)-[2-R_{m,n+1}-R_{m,n-1}]E_y(m,n)+T_{m,n-1}E_y(m,n-1)}{(\Delta y)^2}+\frac{E_y(m+1,n)-2E_y(m,n)+E_y(m-1,n)}{(\Delta x)^2}+[n^2(m,n,l)-n_0^2]k_0^2E_y(m,n)\right\}$$

and so we obtain the following equation:

$$\begin{aligned} (1+\mathrm{j}\Delta z\alpha A_{xx})E_x^{l+1} &= [1-\mathrm{j}\Delta z(1-\alpha)A_{xx}]E_x^l \\ (1+\mathrm{j}\Delta z\alpha A_{yy})E_y^{l+1} &= [1-\mathrm{j}\Delta z(1-\alpha)A_{yy}]E_y^l \end{aligned} \tag{4}$$

where parameter α is introduced to control the schemes for solving the finite difference equations. The discrete formula for the magnetic field components have been derived and can be also found in Ref. [11]. The system of equations based on the Crank-Nicholson approach is not tridiagonal, and requires $O(N_x^2 \cdot N_y^2))$ operations to solve. The help of alternation direction implicit (ADI) method[13] allows the 3D problem to be solved with optimal $O(N_x \cdot N_y)$ efficiency[14]. The equations of the standard ADI scheme are as follows:

$$\begin{aligned} \frac{E_x^{l+1}-E_x^l}{\Delta z} &= (A_x+A_y)\frac{E_x^{l+1}-E_x^l}{2} \\ \frac{E_y^{l+1}-E_y^l}{\Delta z} &= (B_x+B_y)\frac{E_x^{l+1}-E_x^l}{2} \end{aligned} \tag{5}$$

where

$$A_xE_x = -\frac{\mathrm{j}}{2n_0k_0}\left\{\frac{T_{m+1,n}E_x(m+1,n)-[2-R_{m+1,n}-R_{m-1,n}]E_x(m,n)+T_{m-1,n}E_x(m-1,n)}{(\Delta x)^2}\right.$$

$$+\frac{1}{2}[n^2(m,n,l)-n_0^2]k_0^2E_x(m,n)\Big\}$$

$$A_yE_x=-\frac{\mathrm{j}}{2n_0k_0}\left\{\frac{E_x(m,n+1)-2E_x(m,n)+E_x(m,n-1)}{(\Delta y)^2}+\frac{1}{2}[n^2(m,n,l)-n_0^2]k_0^2E_x(m,n)\right\}$$

$$B_yE_y=-\frac{\mathrm{j}}{2n_0k_0}\left\{\frac{T_{m,n+1}E_y(m,n+1)-[2-R_{m,n+1}-R_{m,n-1}]E_y(m,n)+T_{m,n-1}E_y(m,n-1)}{(\Delta y)^2}\right.$$

$$\left.+\frac{1}{2}[n^2(m,n,l)-n_0^2]k_0^2E_y(m,n)\right\}$$

$$B_xE_y=-\frac{\mathrm{j}}{2n_0k_0}\left\{\frac{E_y(m+1,n)-2E_y(m,n)+E_y(m-1,n)}{(\Delta x)^2}+\frac{1}{2}[n^2(m,n,l)-n_0^2]k_0^2E_y(m,n)\right\}$$

adding higher order terms $\left(\frac{\Delta z}{2}\right)^2 A_xA_y$ and $\left(\frac{\Delta z}{2}\right)^2\times B_xB_y$ in Eq.(5), we find:

$$\begin{aligned}&\left(1-\frac{\Delta z}{2}A_x\right)\left(1-\frac{\Delta z}{2}A_y\right)E_x^{l+1}\\&=\left(1+\frac{\Delta z}{2}A_x\right)\left(1+\frac{\Delta z}{2}A_y\right)E_x^{l}\\&\left(1-\frac{\Delta z}{2}B_x\right)\left(1-\frac{\Delta z}{2}B_y\right)E_y^{l+1}\\&=\left(1+\frac{\Delta z}{2}B_x\right)\left(1+\frac{\Delta z}{2}B_y\right)E_y^{l}\end{aligned}\tag{6}$$

Then, we obtain two tridiagonal equations of the standard ADI form:

$$\begin{cases}\left(1-\frac{\Delta z}{2}A_x\right)E_x^{l+\frac12}=\left(1+\frac{\Delta z}{2}A_y\right)E_x^{l}\\\left(1-\frac{\Delta z}{2}A_y\right)E_x^{l+1}=\left(1+\frac{\Delta z}{2}A_x\right)E_x^{l+\frac12}\end{cases}\\\begin{cases}\left(1-\frac{\Delta z}{2}B_x\right)E_y^{l+\frac12}=\left(1+\frac{\Delta z}{2}B_y\right)E_y^{l}\\\left(1-\frac{\Delta z}{2}A_x\right)E_y^{l+1}=\left(1+\frac{\Delta z}{2}A_y\right)E_x^{l+\frac12}\end{cases}\tag{7}$$

Employing full transparent boundary conditions (TBC) as described in Refs.[15,16], we will get the numerical results of the diluted waveguide.

3 Waveguide structure and mode simulation

The diluted waveguide, also called a fiber-to-waveguide coupler, is a kind of waveguide composed of multiple InP/InGaAsP/InP waveguides with weak optical confinement, as presented in Fig. 1. The electromagnetic fields in the diluted waveguide are (E_x, H_y, H_z) and (H_x, E_y, E_z) for TE and TM mode, respectively. Index distribution is quite different along the x-direction and the y-direction. In the x-direction, index distribution is uniform and in the y-direction, index distribution is periodical. In a single InP/InGaAsP/InP plane waveguide, the boundary conditions for the electric field components of TE and TM mode in the x-y plane are so different that the optical fields distributions (electric component) are significantly different. The coupling efficiency of fiber-to-waveguide is decided by the overlap integral between the normalized optical field of a single mode fiber $\Psi(x,y)$ and the normalized optical field of waveguide $\phi_{ij}(x,y)$[1]:

$$\eta_c=\sum_{ij}\left|\iint\Psi(x,y)\phi_{ij}(x,y)\mathrm{d}x\mathrm{d}y\right|^2\tag{8}$$

where i and j are the orders of modes in waveguide in the x- and y-directions, respectively. As a result, the polarization dependence phenomenon of fiber-to-waveguide coupling appears. But, in a diluted waveguide, which is composed of multiple InP/InGaAsP/InP waveguides, the guide modes are formed by strong coupling between the optical fields in individual waveguides. For TE mode, although the electric field component is along the x-direction with uniform index distribution, due to the thin InP separate layers, there are strong evanescent fields of the E_x component in the y-direction. Therefore, the coupling between the E_x component field occurs and forms the TE mode of the diluted waveguide. For TM mode, the electric field component, which is perpendicular to the epitaxial growth direction, is along the y-direction with a step-like refractive index distribution, and therefore the evanescent field coupling is much stronger than in TE mode.

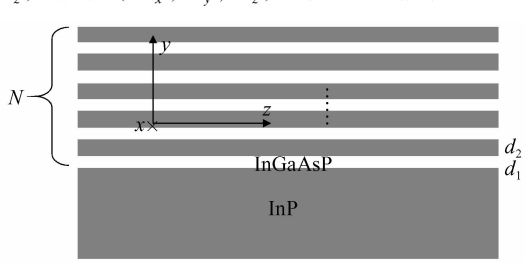

Fig. 1　Schematic of cross section for waveguide structure of the diluted waveguide, grown on a semi-insulating InP substrate, with a period of N　d_1 and d_2 stand for the thickness of InGaAsP and InP respectively.

The optical fields of the guide modes in the diluted waveguide were calculated with the imaginary distance BPM (ID-BPM)[17~19]. We ignored the imaginary part of the refractive indices and set them to be 3.146 for InP and 3.28 for $In_{0.88}Ga_{0.12}As_{0.26}P_{0.74}$ (Q1.05)[20] at the wavelength of 1.55μm. We can choose a set of Gaussian functions $\Phi_m(x,y)$[17] as the eigenfunctions to expand the modes of the diluted waveguides as follows, $\Psi_{\mathrm{in}}(x,y,0)=\sum_m c_m\phi_m(x,y)$,

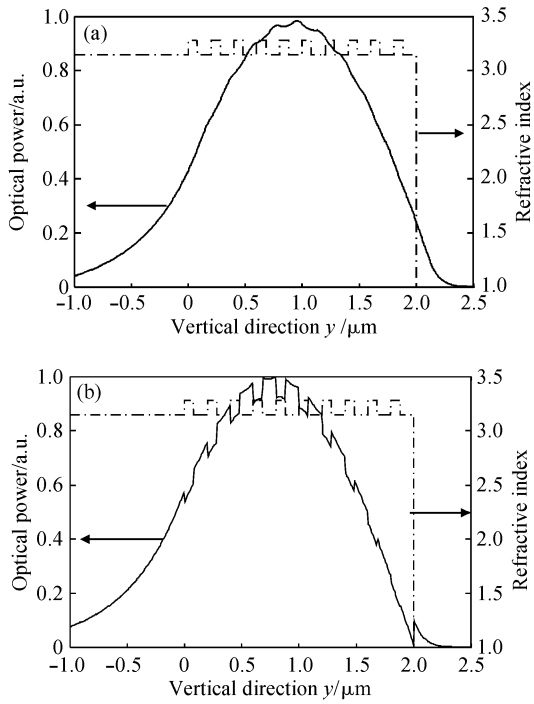

Fig. 2 Distribution of TE fundamental mode field (a) and TM fundamental mode field (b) in the diluted waveguide with ten periods of 120nm/80nm InGaAsP (Q 1.05μm)/InP

where $\Psi_{in}(x,y,0)$ is the incident field to excite guide modes. The propagation can be expressed as $\Psi_{in}(x,y,z)=\sum_m c_m\phi_m(x,y)e^{-i\beta_m z}$, as the name implies, the longitudinal coordinate z is replaced by $\mathrm{Im}z=iz$, and so the propagation along the imaginary axis should follow $\Psi(x,y,\mathrm{Im}z)=\sum_m c_m\phi_m(x,y)e^{\beta_m \mathrm{Im}z}$. Since the fundamental mode has the highest propagation constant by definition, the fundamental mode always dominates after a sufficiently long propagation, and the fundamental mode propagation constant can be obtained by the variational type expression $\beta^2=\frac{\int\Psi^*[k_0^2n^2(x,y)\Psi+\partial\Psi/\partial x+\partial\Psi/\partial y]\mathrm{d}x\mathrm{d}y}{\int\Psi^*\Psi\mathrm{d}x\mathrm{d}y}$. The calculation results of the optical field distribution of TE and TM fundamental modes based on the ID-BPM are shown in Fig. 2. They are of similar envelope despite small variations due to evanescent field coupling. These small variations have little effect on the coupling efficiency and can be neglected. Thus, the fiber-to-waveguide coupler is of low polarization dependence. In addition, the $1/e$ optical field is confined in the diluted waveguide with ten periods of InP/InGaAsP. Using an orthogonalization procedure[21], we can obtain a higher order modes propagation constant and then find all the guided modes of the diluted waveguide, as shown in Fig. 3. The diluted waveguide has a thickness of only 2μm, thus there is only a fundamental mode in the y-direction. Therefore, in

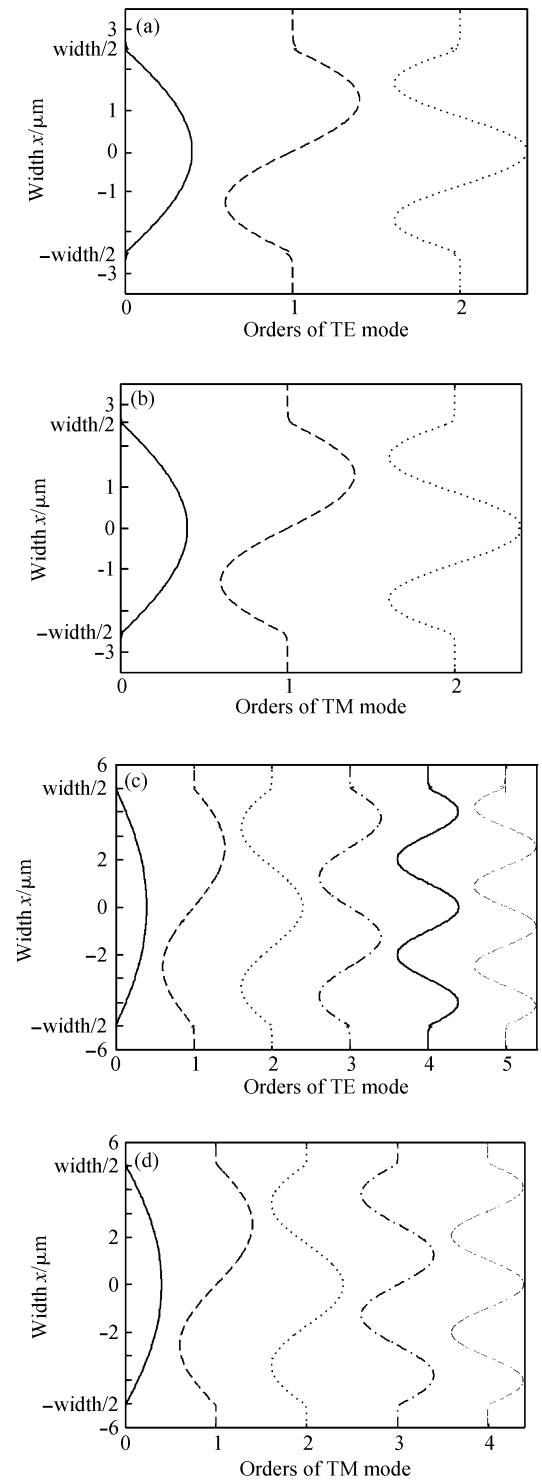

Fig. 3 Calculated optical fields distribution along x-direction with a width of 5μm (a), (b) and 10μm (c), (d) for TE and TM modes respectively

Eq. (8), the y-direction mode order $j=0$. In the x-direction, the calculated optical fields with different orders of modes are presented in Fig. 3. There are three modes when the diluted waveguide is of 5μm width for both TE and TM modes [Figs. 3 (a), 3(b)], while with a diluted waveguide width of 10μm, there are six modes for TE and five for TM modes [Figs. 3 (c), 3(d)] respectively. We will show that these modes have a

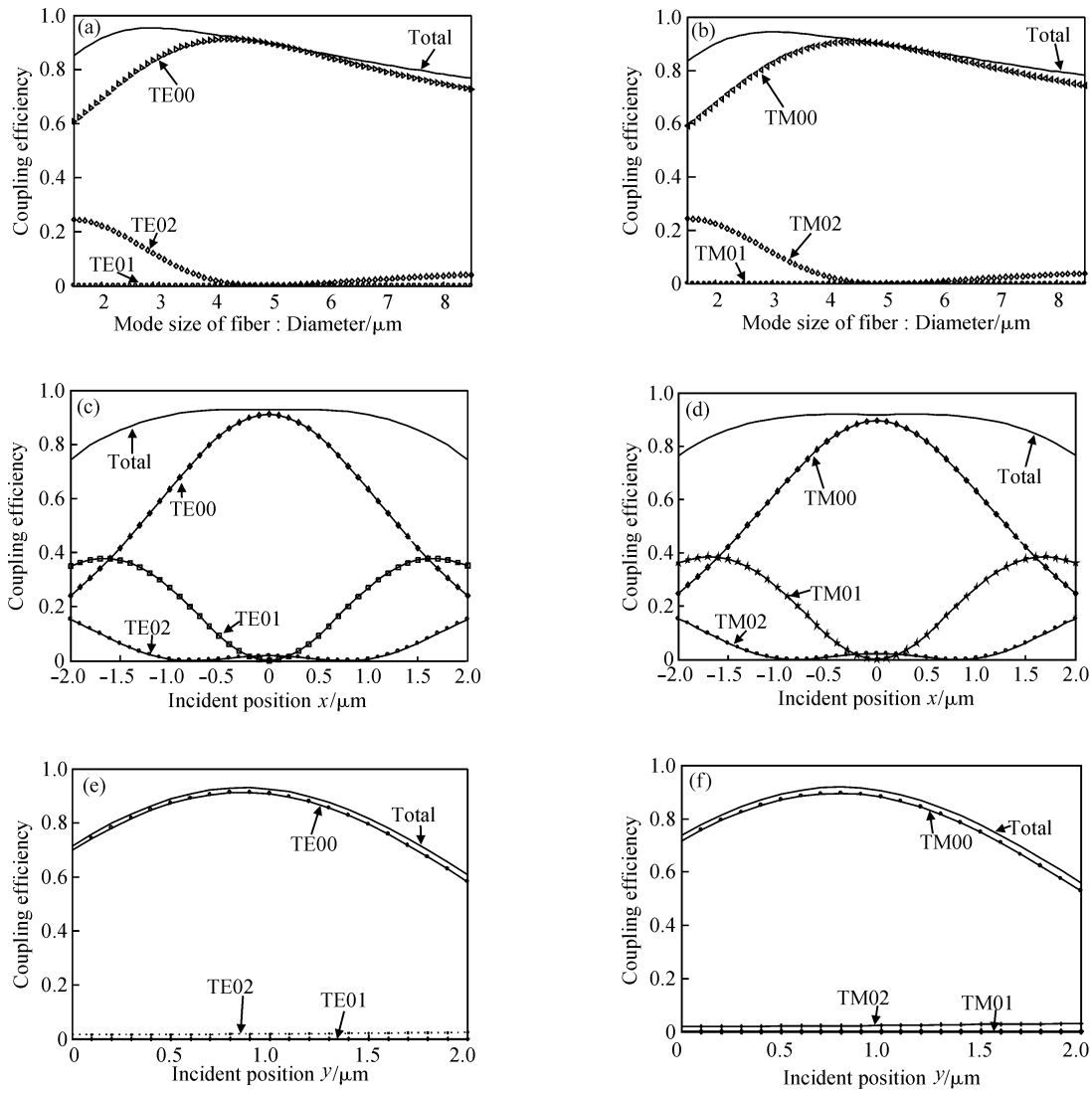

Fig. 4　Calculated fiber-to-waveguide coupling efficiencies with a diluted waveguide width of 5μm　(a), (b) The coupling efficiency varies with the fiber mode size D, with the center of incident light position being (0, 1); (c), (d) The coupling efficiency varies with the incident position in the x-direction, with the center of incident light position being (x, 1), $D = 4$; (e), (f) The coupling efficiency varies with the incident position in the y-direction while the center of incident light position is (0, y), $D = 4$, for TE and TM modes, respectively　Comparing the coupling efficiency of TE mode with TM mode, the polarization dependence is smaller than 0.1dB.

great influence on fiber-to-waveguide coupling in the next section.

4　Fiber-to-waveguide coupling

In order to simulate the coupling of single mode fiber-to-waveguide, we choose an optical field with the Gaussian distribution, $\Psi(x, y) = e^{-\frac{x^2}{(D/2)^2}} e^{-\frac{y^2}{(D/2)^2}}$, as the input single mode fiber mode field to calculate the overlap integral with the modes of diluted waveguide from Eq. (8), where D is the mode size of the output light from a single mode fiber. We calculate the fiber-to-waveguide coupling efficiencies, which vary with the diameters D and the incident position in the x- and y-direction, respectively, at the widths of 5μm and 10μm without considering the reflection of the incident facet. The results are represented as follows.

The diluted waveguide with a width of 5μm reaches the highest coupling efficiency (>94%) with the mode size of 2.9μm for TE mode and 3μm for TM mode, as shown in Figs. 4 (a) and 4 (b). The odd modes have no contribution to the coupling efficiency, because the optical field of the odd mode is zero in the y-z plane at $x = 0$, shown in Fig. 3. The coupling efficiency is mainly decided by the fundamental mode. Due to the multimode in the x-direction, the coupling efficiencies of higher order modes vary periodically with the incident position x, shown in Figs. 4 (c) and 4 (d), and the total coupling efficiency, the summation of the individual mode's, is quite flat and

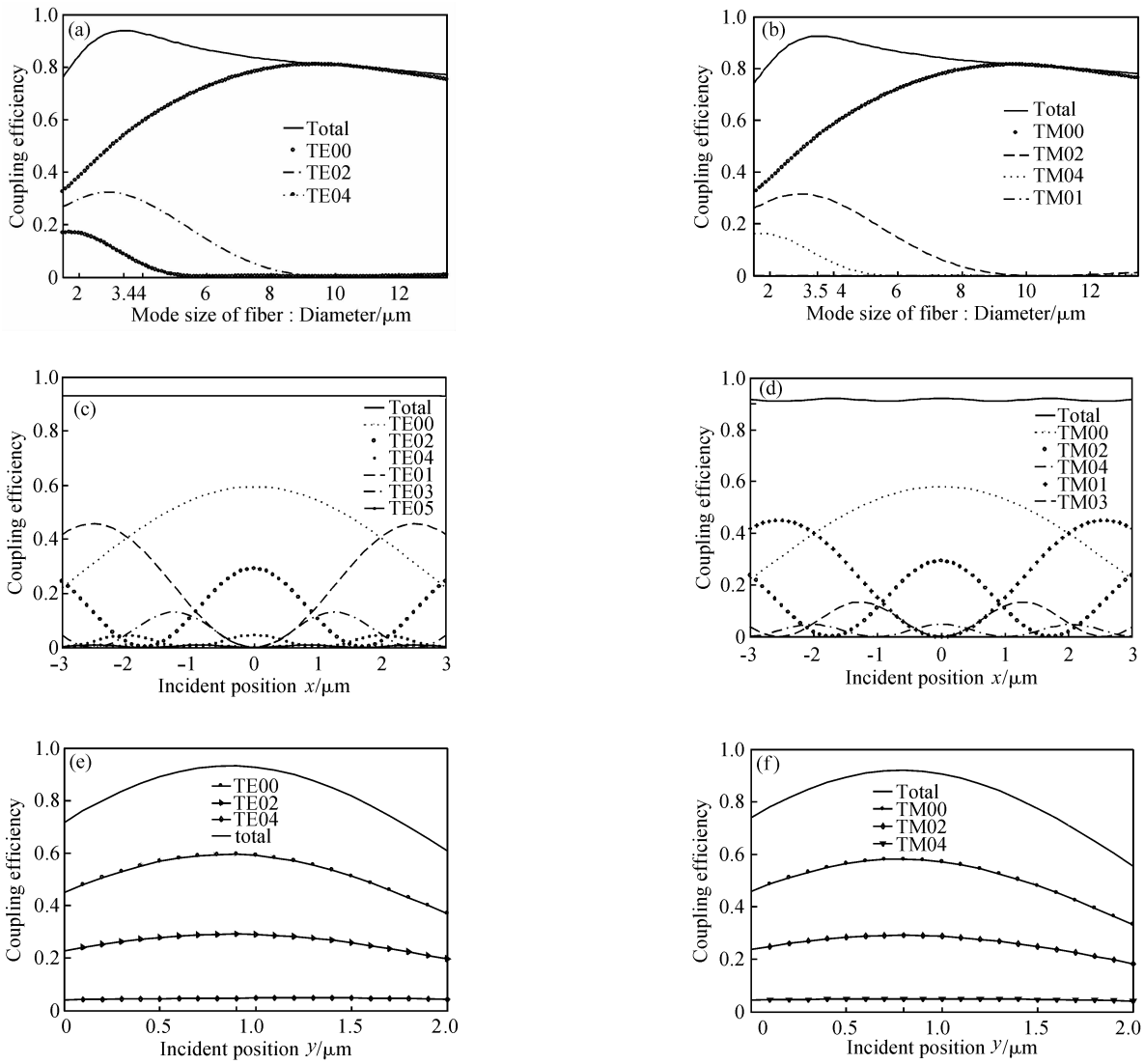

Fig. 5 Calculated fiber-to-waveguide coupling efficiencies with a diluted waveguide width of 10μm (a), (b) The coupling efficiency varies with the fiber mode size D, center of the incident position (0, 1); (c), (d) The coupling efficiency varies with the incident position in x-direction, center of the incident position (x, 1), $D = 4$; (e), (f) The coupling efficiency varies with the incident position in y-direction center of incident position (0, y), $D = 4$, for TE and TM modes, respectively Comparing the coupling efficiency of TE mode with TM mode, the polarization dependence is smaller than 0.1dB.

has good incident tolerance in the x-direction. In the y-direction, the diluted waveguide is not symmetric and the optical field expands to the InP substrate to some extent, and the center position of the mode is around $y = 0.8$ (see Fig. 2). Thus, the optimal position for incident is not $y = 1$ but $y = 0.9$ for TE mode and $y = 0.8$ for TM mode, as shown in Figs. 4 (e) and 4 (f).

For the coupling efficiency curves versus the fiber mode size D, the center position of incident light x and y when the diluted waveguide width is 10μm are similar to the curves when the width is 5μm. Because there are more modes than the waveguide with 5μm width, as presented in Fig. 3, the coupling efficiency varying with x is nearly constant and the coupling efficiencies of higher order modes are periodical, as shown in Figs. 5 (c) and 5(d). Figures 5 (a) and 5(b) show that the optional mode size D for fiber-to-waveguide coupling is 3.4μm for TE mode and 3.5μm for TM mode, with a coupling efficiency of more than 92%, smaller than the 5μm width waveguide's. This is because the mode spot with a 10μm width waveguide expands more than the 5μm width waveguide in the x-direction, as shown in Fig. 6 (a).

The field distributions within $1/e$ width of Gaussian modes and 5μm-width waveguide fundamental modes almost overlap in the x-direction, and the fundamental mode of the 10μm-width has a much larger mode spot and smaller overlap. At the same time, in the y-direction, the waveguide modes have the same field distribution, (see Fig. 6 (b)), regardless of the polarization and waveguide width.

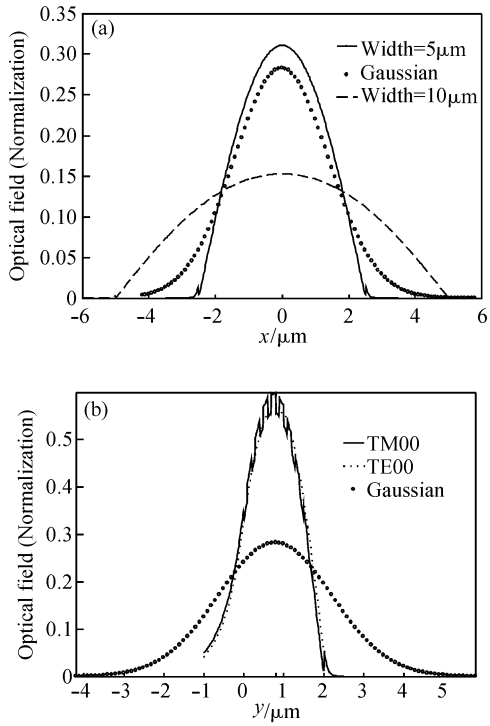

Fig. 6　Optical field distributions of the Gaussian mode (D = 4μm), TE fundamental modes with widths of 5μm, 10μm along x-direction (a), and the Gaussian mode (D = 4μm), TE and TM mode field distribution along the y-direction (b)

Table 1　Calculated fiber-to-diluted waveguide coupling performance

Waveguide width/μm	5	10
Coupling efficiency/%	95	93
Polarization dependence (TE/TM, maximum)/dB	0.08	0.1
−1dB alignment (Δy, D = 4μm)/μm	±0.8	±0.7

5　Conclusion

We have proposed a multimode diluted waveguide as a fiber-to-waveguide coupler. Using the imaginary distance BPM, we calculated all the guide modes of the waveguide with widths of 5 and 10μm, respectively. The simulation results explain theoretically why the coupler is of low polarization dependence. Taking a Gaussian mode as the single fiber mode, the coupling efficiencies of individual modes were obtained by overlap integral and used to find the optimal coupling condition: fiber mode size about 3μm for the waveguide with a width of 5 and 3.5μm for the waveguide with a width of 10μm, and the center position of incident light is about (0, 0.8). These simulation results show that the coupler can provide quite relaxed tolerances and perfect coupling performances (see Table 1). The polarization dependence is lower than 0.1dB and the coupling efficiency is higher than 90%, up to 95% for waveguide with a width of 5μm and 93% for waveguide with a width of 10μm in the optimal conditions. Therefore, we conclude that diluted waveguides could provide a useful way for realizing fiber-to-waveguide couplers with high coupling efficiency and low polarization dependence that are compatible with hybrid optoelectronics integration.

References

[1] Kato K, Hata S, Kawamo K, et al. A high-efficiency 50GHz InGaAs multimode waveguide photodetector. IEEE J Quantum Electron, 1992, 28: 2728

[2] Bowers J E, Burrus C A. Ultrawide-band long-wavelength p-i-n photodetectors. J Lightwave Technol, 1987, LT-5: 1339

[3] Demiguel S, Giraudet L, Joulaud L, et al. Evanescently coupled photodiodes integrating a double-stage taper for 40-Gb/s applications-compared performance with side-illuminated photodiodes. J Lightwave Technol, 2002, 20: 2004

[4] Sarathy J, Anselm K A, Streetman B G, et al. Narrow linewidth, tunable distributed feedback photodetector. Appl Phys Lett, 1996, 69: 3123

[5] Demiguel S, Li N, Li X, et al. Very high-responsivity evanescently coupled photodiodes integrating a short planar multimode waveguide for high-speed applications. IEEE Photonics Technol Lett, 2003, 15: 1761

[6] Achouche M, Magnin V, Harari J, et al. High performance evanescent edge coupled waveguide unitraveling-carrier photodiodes for >40-Gb/s optical receivers. IEEE Photonics Technol Lett, 2004, 16: 584

[7] Wu Y S, Shi J W, Huang F H, et al. High-performance evanescently edge coupled photodiodes with partially p-doped photoabsorption layers at 1.55-μm wavelength. IEEE Photonics Technol Lett, 2005, 17: 878

[8] Huang W K, Huang S C, Chung H W, et al. 37-GHz bandwidth monolithically integrated InP HBT/evanescently coupled photodiode. IEEE Photonics Technol Lett, 2006, 18: 1323

[9] Magnin V, Giraudet L, Harari J, et al. Design, optimization, and fabrication of side-illuminated p-i-n photodetectors with high responsivity and high alignment tolerance for 1.3-μm wavelength use. J Lightwave Technol, 2002, 20: 477

[10] Shi J W, Wu Y S, Wu C Y, et al. High-speed, high-responsivity, and high-power performance of near-ballistic uni-traveling-carrier photodiode at 1.55-μm wavelength. IEEE Photonics Technol Lett, 2005, 17: 1929

[11] Huang W P, Xu C L. Simulation of three-dimensional optical waveguides by a full-vector beam propagation method. IEEE J Quantum Electron, 1993, 29: 2639

[12] Xia Jinsong. Numerical simulation and fabrication of optical waveguide switch in silicon-on-insulator. PhD Dissertation, Graduate School of the Chinese Academy of Sciences, 2003

[13] Hsueh Y L, Yang M C, Chang H C. Three-dimensional noniterative full-vectorial beam propagation method based on the alternating direction implicit method. J Lightwave Technol, 1999, 17: 2389

[14] Yamauchi J, Ando T, Nakano H. Beam-propagation analysis of optical fibers by alternating direction implicit method. Electron Lett, 1991, 27: 1663

[15] Ronald Hadley G. Transparent boundary condition for the beam propagation method. IEEE J Quantum Electron, 1992, 28: 363

[16] Ronald H G, Smith R E. Full-vector waveguide modeling using an iterative finite-difference method with transparent boundary conditions. J Lightwave Technol, 1995, 13: 465

[17] Jungling S, Chen J C. A study and optimization of eigenmode calculations using the imaginary-distance beam-propagation method.

IEEE J Quantum Electron,1994,30:2098
[18] He Y Z, Shi F G. Finite-difference imaginary-distance beam propagation method for modeling of the fundamental mode of photonic crystal fibers. Elsevier Optics Communications, 2003, 225:151
[19] Yevick D, Bardyszewski W. Correspondence of variational finite-difference (relaxation) and imaginary-distance propagation methods for modal analysis. Opt Lett,1992,17:329
[20] http://www.luxpop.com/
[21] Chen J C, Jungling S. Computation of higher-order waveguide modes by imaginary-distance beam propagation method. Springer Optical and Quantum Electronics,1994,26:199

基于稀释波导的 InP 衬底上高耦合效率、低偏振敏感度 1.55μm 波长光纤-波导耦合器*

张 云 左玉华† 郭剑川 丁武昌 成步文 余金中 王启明

(中国科学院半导体研究所 集成光电子国家重点实验室, 北京 100083)

摘要: 研究了一种用于边入射型探测器的 InP 基高效光纤-波导耦合器.它由 10 个周期的未掺杂 120nm InP/80nm InGaAsP (1.05μm 带隙)多层膜组成的稀释波导构成.采用半矢量三维束传播(BPM)方法以及中心差分格式,模拟了不同条件下的光纤-波导耦合效率,从而得到了最优耦合条件.对于 TE 偏振和 TM 偏振模,计算所得到的最高耦合效率分别为 94%和 92%.同时,计算表明,此类基于稀释波导的光纤-波导耦合器具有高偏振不敏感性,偏振敏感度低于 0.1dB.

关键词: 稀释波导; 束传播方法; 光纤-波导; 波导型探测器
PACC: 4281M **EEACC**: 4130
中图分类号: O472$^+$.3 **文献标识码**: A **文章编号**: 0253-4177(2008)01-0055-08

* 国家高技术研究发展计划资助项目(批准号:2006CB302802)
† 通信作者.Email:yhzuo@red.semi.ac.cn
2007-07-09 收到,2007-08-21 定稿